

The upper talocalcanean joint

B. Odehnal H. Stachel

October 2004

Abstract

The upper talocalcanean joint (articulatio talocruralis)¹ is the joint of the shin bone (tibia) and the ankle bone (talus). The tibia and the ankle bone are in contact at the facies articularis inferior tibiae² and the facies articularis superior trochleae tali³. In order to build prostheses that simulate the motion of the UTJ we study the geometry of the two surfaces FAIT and FAST, respectively. We are looking for kinematic surfaces that approximate FAIT and FAST best. For that we use line geometric methods to fit best approximating linear line complexes and compute the axis of the thus determined helical motion.

Further we register FAIT and FAST in order to find configurations such that they are in contact. Measuring deviations of the registered surfaces helps to decide if FAIT and FAST can be in line contact. The detection of possible contact curves will be a topic of future research.

Keywords: shin bone, ankle bone, line geometry, linear line complex, helical motion, surface reconstruction, registration, surface normals, complex fitting.

Mathematics Subject Classification (AMS 2000): 53A05, 53A17, 70B10

1 Introduction

The UTJ is known as a cylindrical joint (ginglymus), see [8, 14]. Unfortunately prostheses with cylindrical shape do not simulate the motion of the ankle bone

¹In the following we use the abbreviation UTJ.

²For short: FAIT.

³For short: FAST.

relatively to the shin bone very well. So it is obvious to study the geometry of the surfaces FAIT and FASTT which are in contact during the motion. The shape of FAIT and FASTT, respectively, determines or at least constrains the motion of the UTJ.

In Euclidean space there are exactly three types of surfaces which are invariant under Euclidean motions: cylinders, rotational surfaces and helical surfaces. Assuming that FAIT and FASTT are in contact in all points of a certain region they can only be one of these three types of surfaces.

Since cylinders, rotational and helical surfaces allow a kinematic generation, i.e., they are swept by a curve under a translation, rotation or helical motion, they are called *kinematic surfaces*. Surfaces of that kind can easily be recognized by their set of surface normals. It is well known (see e.g. [13]) that the *congruence of surface normals* of a kinematic surface is contained in a *linear line complex*. This gives a tool for recognition of kinematic surfaces which has been of use, e.g. in [9, 12, 13].

The surfaces we have in mind - FAIT and FASTT, respectively - are represented by noisy point clouds. This 3D data is obtained by a Minolta Vivid 900 3D laser scanner. Noise can be reduced with subdivision techniques and other algorithms. Normals to the points of the triangulated surfaces are estimated locally by means of regression planes. The RANSAC principle [1] and improvements of normal estimation methods [7] are very useful.

The paper is organized in the following way: In Sec. 2 we summarize basic results on line geometry and kinematics. Sec. 3 is dedicated to a detailed description of the methods and algorithms used in the experimental part in Sec 4. The results produced by our algorithms are presented in Sec. 4. Finally we conclude and discuss improvements and future research in Sec. 5.

2 Fundamentals of line geometry

2.1 Coordinates of lines

In this section we summarize well known facts and result from line geometry as far as needed in order to understand the methods and algorithms in the present paper. The interested reader is referred to [4, 5, 6, 13, 15].

We represent points p in Euclidean three-space \mathbb{R}^3 by Cartesian coordinates $p = (p_1, p_2, p_3)$. An oriented line L in Euclidean three-space \mathbb{R}^3 can be

uniquely represented by *normalized Plücker coordinates*. Let p be a point on L and let l be a unit vector parallel to L then the vector $\bar{l} := x \times l$ is called *momentum vector* of L and the six tuple (l, \bar{l}) comprises the Plücker coordinates of L .

Obviously, the Plücker coordinates of lines are independent on the choice of p on L . The direction vector l and momentum vector \bar{l} of a line are perpendicular and so we have

$$\langle l, \bar{l} \rangle = 0, \quad (1)$$

which will be called the *Plücker relation*. Here and in the following $\langle x, y \rangle$ denotes the standard scalar product of vectors x and y , respectively. Any six tuple (l, \bar{l}) of real numbers which satisfies (1) can be interpreted as the coordinates of a line in Euclidean three-space. Thus there is a one-to-one correspondence between oriented lines in Euclidean three-space and the points of a four-dimensional algebraic manifold M^4 in \mathbb{R}^6 , which is given by the equations

$$\langle l, \bar{l} \rangle = 0, \quad \langle l, l \rangle = 1. \quad (2)$$

Assume S is a surface having only regular points, i.e., we can compute a tangent plane in each of its points or equivalently we can compute its (arbitrarily oriented) normal $N = (n, \bar{n})$. The two-dimensional manifold of surface normals is usually called the *congruence of surface normals* of S . The assignment of Plücker coordinates to all the surface normals transforms the congruence of surface normals to a two-dimensional submanifold of M^4 .

2.2 Linear line complex of path normals

A Euclidean motion transforms points $x \in \mathbb{R}^3$ according to $x \mapsto y = Ax + a$, where A is an orthogonal matrix and a is a vector in \mathbb{R}^3 . Assume for a moment that A and a depend on a parameter t and assume further that all coordinate functions are at least one times differentiable. Then the velocity of a point y can be computed by

$$v(y) = \dot{A}x + \dot{a} = \dot{A}A^T y + \dot{a} - \dot{A}A^T a = c \times y + \bar{c}. \quad (3)$$

Because of A 's orthogonality we have $AA^T = E_3$, where $E_3 = \text{diag}(1, 1, 1)$. Differentiating this latter identity we find $\dot{A}A^T + (\dot{A}A^T)^T = 0$ which reveals the skew-symmetry of $\dot{A}A^T$ and the product $\dot{A}A^T y$ can be written as $c \times y$ as done in (3).

The field of velocity vectors of a Euclidean motion thus depends linearly on the points of \mathbb{R}^3 . Assume $L = (l, \bar{l})$ is a path normal of point y , i.e. it is normal to $v(y)$. So we have

$$0 = \langle v(y), l \rangle = \langle c \times y + \bar{c}, l \rangle = \det(c, y, l) + \langle \bar{c}, l \rangle = \langle c, \bar{l} \rangle + \langle \bar{c}, l \rangle =: \Omega(C, L). \quad (4)$$

Equ. (4) obviously is a linear homogeneous equation in the Plücker coordinates of the path normal L . The set of lines whose Plücker coordinates satisfy a homogeneous linear equation is called *linear line complex* \mathcal{C} . The six-tupel (c, \bar{c}) is a coordinate vector of \mathcal{C} .

In case of $\langle \bar{c}, c \rangle \neq 0$ \mathcal{C} is called *regular linear line complex*. It is well known that any regular linear line complex consists of the path normals of a certain helical motion with axis $A = (a, \bar{a}) = (c, \bar{c} - pc) / \|c\|$, where $p = \langle \bar{c}, c \rangle / \langle c, c \rangle$ is the so-called *pitch* of the helical motion.

If $\langle \bar{c}, c \rangle = 0$ the linear line complex \mathcal{C} is called *singular*. It consists of all lines intersecting a single straight line C called axis, whose normalized Plücker coordinates are a multiple of C .

The discussion of the right hand side of (3) leads to the different types of Euclidean motions with time independent velocity field. The following three types can be distinguished (cf. [6, 13]):

1. $\langle \bar{c}, c \rangle \neq 0$ corresponds to a *helical motion*.
2. $\langle \bar{c}, c \rangle = 0$ and $c \neq 0$ describes the set of path normals of a *rotation*. This set of lines is known to meet the axis.
3. $c = 0$: In this case the path normals are arranged in parallel planes. Projectively speaking they meet a line at infinity. In this case the motion is a *translation*.

3 The algorithms

3.1 Complex fitting

In the following we look for linear line complexes that contain given lines. In general five independent lines determine a linear line complex. Now we are given finitely many lines (in Sec. 4 we deal with approximately 10000 points and normals) of the congruence of normals of a surface S .

A closer look to Equ. (4) shows that in our setting linear line complexes are represented by hyperplanes of \mathbb{R}^6 . Since Equ. (4) is homogeneous the hyperplane defined by a linear line complex passes through the origin of the coordinate system.

To fit a linear line complex $C = (c, \bar{c})$ to a set of given lines $\{L_i\}$ ($i = 1, \dots, n < \infty$) thus means find a hyperplane H that passes through the origin of the coordinate system and minimizes the sum of squared distances of data points to it. Distances in our model of line space are measured with the metric induced by (4) since $\Omega(X, Y) = 0$ means X is contained in Y . Consequently the system of normal equations of the present LQ-problem is given by

$$\begin{bmatrix} \sum_{i=1}^n \bar{l}_i \cdot \bar{l}_i^T & \sum_{i=1}^n \bar{l}_i \cdot l_i^T \\ \sum_{i=1}^n l_i \cdot \bar{l}_i^T & \sum_{i=1}^n l_i \cdot l_i^T \end{bmatrix} \begin{bmatrix} c \\ \bar{c} \end{bmatrix} = MC = 0. \quad (5)$$

This system of homogeneous linear equations is solvable if and only if the 6×6 -matrix M is singular. Thus the approximating linear line complex to L_i corresponds to the eigenvector of the smallest eigenvalue of M .

If M has $k > 1$ small eigenvalues the set of given surface normals is contained in k independent linear line complexes. For example: If the set of data comes from a sphere the normals form a bundle of line, i.e. they are concurrent in the center of the sphere. In this case M has three small eigenvalues.

We can refine the computation of the linear line complex by assigning weights to the lines. Let L_i be the normal at point p_i of the triangulated point cloud. Let further t_i be the list of triangles sharing the vertex p_i . Compute the sum of the area of all triangles in t_i and divide by the number of triangles in t_i . We choose this kind of weight if the data is not uniformly sampled.

If data is uniformly sampled, i.e. the triangles have approximately equal size we prefer another kind of weight. First we compute a linear line complex as eigenvector to the smallest eigenvalue of M from (5). Then we can assign the *momentum of a line L with respect to a linear line complex C* to L . It is defined by

$$\mu(L, C) = \Omega(L, C), \quad (6)$$

where C is normalized such that $\|c\| = 1$. It is elementary to verify that for a line L with normalized Plücker coordinates the identity $\mu(C, L) =$

$p \cos \phi - d \sin \phi$ between the distribution parameter p of C , the distance d of L and the axis A of C and the angle ϕ enclosed by L and A holds.

The momentum equals zero for lines in the complex. The momentum is approximately zero for lines that fit well into C ; it becomes large for those lines that do not fit very well. A *weight function* like

$$w(L_i) = \frac{1}{1 + \mu(L_i, C)^r}, \quad (7)$$

with positive even r punishes lines that do not fit well into C . Weights enter the computation by multiplying the Plücker coordinates of L_i with $w_i(L_i)$.

Finally we repeat the computation of C and weights until the sum of squared moments falls under a predefined threshold.

3.2 Reconstruction of kinematic surfaces

We want to create a geometric model of a surface that is given by scattered data. So we compute the best fitting linear line complex to the set of surface normal. Now we recognize the given surface as one of the three types of kinematic surface. We do already know that kinematic surfaces admit a kinematic generation, i.e. there exists a Euclidean motion such that the given surface is swept by a curve.

In order to find a curve with the required property, we apply the motion corresponding to the best approximating linear line complex $C = (c, \bar{c})$ to the surface points. We move them until their paths hit a certain plane, e.g. a plane through the axis. The thus obtained set of points forms a fat curve m_f , points are distributed in a small region around a curve if the surface admits a kinematic generation. Now a smooth curve m needs to be computed such that it is not too far from m_f . There are a lot of algorithms for that, see [10, 3, 2]

The thus obtained curve - we call it *meridian* m - can serve as generatrix. With the curve m we are able to rebuild the surface and find a simple CAD model.

3.3 Registration

The registration of the CAD model and the original surface helps to check the quality of the approximation. The aim of registration processes is to

move a surface S_1 onto a surface S_2 in order to show that they are congruent or one is a good approximation of the other. Although there exists software for registration, we need special features.

Usually registration does not care if registered surfaces intersect. Registration algorithms only deal with geometric objects without paying attention to real world. Collision detection is not a topic for registration, though it should be. The surfaces FAIT and FASTT can touch only on specified sides: bones can not touch each other from the interior.

Our registration works as follows: First we choose the sides of the surfaces where the shall come in contact. Then we look for a good starting position of the registration. Now we move S_2 against S_1 until the sum of squared distances falls under a given threshold and S_2 stays on one side of S_1 .

4 Experimental part

In this section we summarize the results of the algorithms applied to original data set. We briefly describe the material and results of the surface recognition and surface reconstruction algorithm. These result may help to decide which shape a talus prothesis should have.

4.1 Material

We obtained data from two left and two right tali and tibiae. The point clouds we dealt with consist of approximately 10000 data points and 20000 triangles. Noise is treated with smoothing subdivision processes. We tried to extract the same area from each compound. In Fig. 1 the areas of interest are marked red. Left hand side of Fig. 1 shows a tibia. Right hand side shows an ankle bone.

4.2 Recognition and reconstruction

The recognition and reconstruction phase for the tibiae leads to the results listed in Tab. 1. In Tab. 1 the pitch p , the number of points and faces of the triangular mesh of FAIT and FASTT are given. The columns w_i show the distribution of surface points or equivalently surface normals with weight

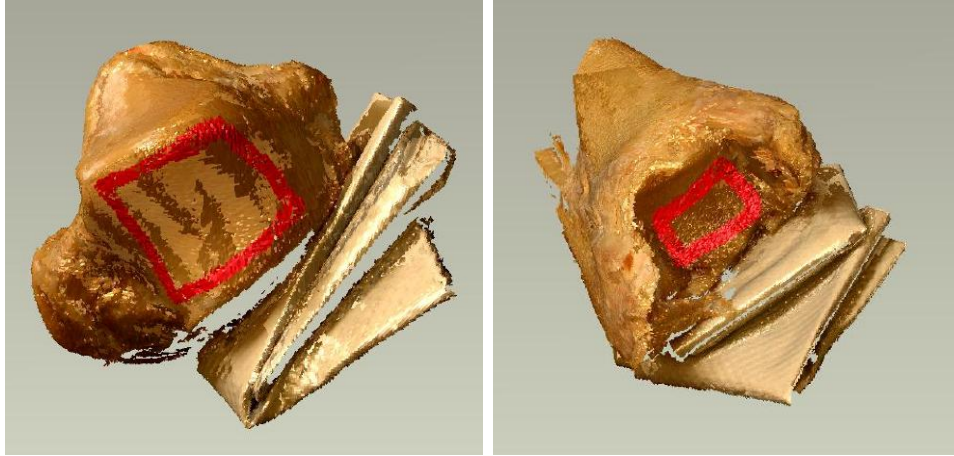


Figure 1: Left: Tibia and area of interest (red). Right: Trochlea tali and area of interest (red).

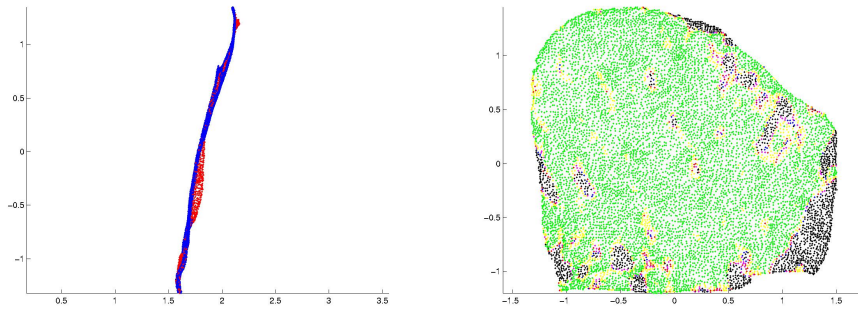


Figure 2: Trochlea tali: meridian curve (left), distribution of points with different weights(right)

in the intervals $w_1 = [1, 0.9[$, $w_2 = [0.9, 0.8[$, $w_3 = [0.8, 0.7[$, $w_4 = [0.7, 0.6[$, $w_5 = [0.6, 0.5[$, $w_6 = [0.5, 0]$. The values in the columns are percentages.

Fig. 2 shows a meridian curve of FASTT₂ on the left. Red dots of the meridian indicate points with weight larger than the mean weight.

The right hand side of Fig. 2 shows the distribution of weights on FASTT₂. Points with weight in the interval w_1 are marked green, points with weights in w_2 are marked yellow, followed by red, magenta, blue and black.

FAIT	p	points	faces	w_1	w_2	w_3	w_4	w_5	w_6
1	0.48665	7099	13825	46.38	11.59	3.47	2.41	2.14	34.01
2	0.33843	6288	12229	42.27	12.64	3.82	2.69	1.49	36.59
3	-0.38172	5748	9837	71.90	9.08	1.81	1.22	1.08	14.01
4	-0.26077	10005	20005	51.19	11.00	3.33	2.16	1.62	30.71
FASTT	p	points	faces	w_1	w_2	w_3	w_4	w_5	w_6
1	-0.18376	10307	20609	53.30	13.12	3.09	2.69	2.04	25.76
2	-0.00097	10255	19695	72.19	10.12	2.16	1.73	0.98	12.82
3	0.07604	7768	13157	86.30	5.14	1.02	0.91	0.58	6.05
4	-0.08407	8316	14356	89.92	6.18	1.02	0.82	0.65	1.49

Table 1: Tibiae and trochleae tali: pitch p , number of points and triangles, distribution of weights after final recursion step.

min	max	mean	dev.	d_1	d_2	d_3	d_4	d_5	d_6
0.1541	10.1722	2.7769	1.9460	6.25	34.62	24.76	10.28	6.65	6.59
0.1394	5.8942	2.6206	0.9542	2.83	17.78	33.92	28.55	14.27	2.65
0.3016	11.9900	3.5202	2.0000	2.02	7.88	18.89	20.87	9.34	5.03
0.7093	6.2404	2.5530	0.9493	0.61	2.72	38.97	24.15	9.16	4.39

Table 2: Tibia and deviations.

4.3 Registration

The results of the registration are listed in Tab. 2. The surfaces FAIT_i are moved towards FASTT_i . At the final position of the registration algorithm the deviations of both surfaces are computed and displayed. We computed the distances of all points in FAIT_i to the surface FASTT_i . Minimum and maximum distances as well as mean and standard deviation of distances are listed in Tab. 2. The percentage rates in columns d_i of Tab. 2 show the relative frequency of points on FAIT_i having a distance $d_1 \in [0, 0.9[$, $d_2 \in [0.9, 1.8[$, $d_3 \in [1.8, 2.7[$, $d_4 \in [2.7, 3.6[$, $d_5 \in [3.6, 4.5[$, $d_6 \in [4.5, \infty[$, where units are Millimeters.

Fig. 3 shows the deviations of FAIT_2 to FASTT_2 . Nearby points are black, followed by blue, magenta, red, yellow, green and empty circles.

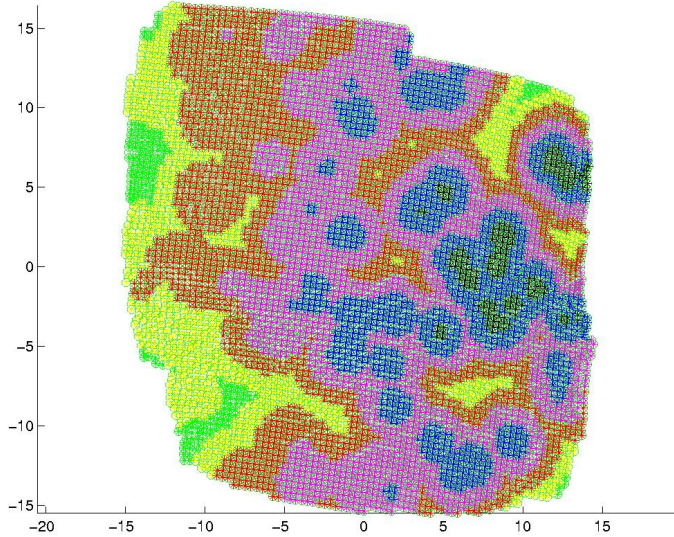


Figure 3: Deviations of FAIT₂ and FASTT₂.

5 Conclusion and future research

The recognition and reconstruction of FASTT and FAIT do not enable general statements on the shape of these two surfaces. As can be seen from the tables the pitch of the helical motion that generates either of the surfaces is sometimes positive, sometimes negative and sometimes close to zero. Consequently more material needs to be studied.

The registration shows that FAIT and FASTT can be brought in contact such that the surfaces agree at least locally in a dense set of points. Taking into account that bones are deformable under pressure, we can say that there could be a two-parametric motion constrained by FAIT and FASTT. This conjecture can only be verified with much more data.

The investigations presented so far did not deal with the case of line contact of FAIT and FASTT. Future research will attack this problem. We have to look for a method to find possible contact curves in either surfaces. If there exists a pair of congruent curves in FAIT and FASTT, respectively, we have to register FAIT and FASTT such that they agree along the contact curve, This results in a starting position for a constrained motion of FAIT against FASTT with permanent line contact during the motion.

6 Acknowledgements

We have to express our sincere thanks to Prof. R. Reimann and G. Windisch from the University of Graz. They confronted us with related problems.

References

- [1] M. A. Fischler, R. C. Bolles: Random Sample Consensus: A Paradigm for Model Fitting with Applications to Image Analysis and Automated Cartography. *Comm. of the ACM*, 24, 1981, 381–395.
- [2] R. L. Graham, P. Hell: On the History of the Minimum Spanning Tree Problem. *Ann. History Comput.* 7, 1985, 43–57.
- [3] R. W. Hamming: *Digital Filters*. Prentice-Hall, 1983.
- [4] J. Hoschek: *Liniengeometrie*. Bibliographisches Institut, Zürich, 1971.
- [5] M. Husty, A. Karger, H. Sachs, W. Steinhilper: *Kinematik und Robotik*. Springer-Verlag, 1997.
- [6] A. Karger, J. Novaák: *Space Kinematics and Lie Groups*. Gordon & Breach Science Publishers, 1985.
- [7] N. J. Mitra, A. Nguyen, L. Guibas: Estimating Surface Normals in Noisy Point Cloud Data. *Int. J. of Comp. Geom. & Applications* 15:13, 2004, 1–17.
- [8] F. H. Netter, J. T. Hansen: *Atlas of Human Anatomy*. Novartis Medical Education, 2002.
- [9] H. Pottmann, M. Hofer, B. Odehnal, J. Wallner: Line Geometry for 3D Shape Understanding and Reconstruction. In: T. Pajdla and J. Matas, eds., *Computer Vision - ECCV 2004, Part I*, volume 3021 of *Lecture Notes in Computer Science*, 2004, 297–309.
- [10] H. Pottmann, S. Leopoldseder, M. Hofer: Approximation with active B-spline curves and surfaces. *Proc. Pacific Graphics 02*, IEEE Computer Society, 2002, 8–25.
- [11] H. Pottmann, S. Leopoldseder, M. Hofer: Registration without ICP, *Computer Vision and Image Understanding* 95(1), 2004, 54–71.

- [12] H. Pottmann, T. Randrup: Rotational and helical surface reconstruction for reverse engineering. *Computing* 60, 1998, 307–322.
- [13] H. Pottmann, J. Wallner: *Computational Line Geometry*. Springer-Verlag, 2001.
- [14] W. Pschyrembel, O. Dornblüth, H. Hildebrandt: *Klinisches Wörterbuch*. 258th edition, de Gruyter, Berlin 1997.
- [15] H. Stachel: Coordinates - A Survey on Higher Geometry. *Computer Networks and ISDN-Systems* 29, 1997, 1645–1654.
- [16] G. Windisch, B. Odehnal, R. Reimann, H. Stachel: Fünf Freiheitsgrade? - In wiefern das obere Sprunggelenk von einem idealen Schanier abweicht, poster session, Würzburg 2004.